Azimuthal Symmetry of the Triaxial Induction Tensor within a VTI Anisotropy Layer Model.

Carvalho, P. R. (ICIBE/UFRA), Régis, C. R. T. (CPGf/UFPA, INCT/GP), Figueiredo, J. J. S. (CPGf/UFPA, INCT/GP) and Silva, V. S. (Campus Castanhal/UFPA).

Abstract

We examine the effects of three relative angles on the nine signals of the triaxial induction tensor: 1) wellbore dip angle, 2) wellbore azimuth angle, and 3) the tool rotation angle around its axis. This study is performed in a basic 1D layered cake model, including vertical transversely isotropic beds (VTI anisotropy), penetrated by an arbitrary LWD trajectory with negligible borehole effects.

Our study shows, geometrically and numerically, that if we fix the values of the wellbore dip angle and the tool rotation angle and vary only the wellbore azimuth angle, the relative positions of the nine coil configurations of the triaxial tools remain constant in relation to the VTI anisotropic medium, which is laterally continuous.

Conclusion, for the sake of clarity and simplification, as well as to improve code efficiency, we recommend ignoring the wellbore azimuth angle in this kind of modeling since it is only important in situations with no azimuthal symmetry, such as those containing vugs, sand/shale lenses, cross-stratifications, fracture zones, and similar features.

Introduction

The introduction of the Ultra Deep Azimuthal Resistivity (UDAR) induction tools towards the beginning of the last decade represents a new generation of Logging While Drilling (LWD) geosteering tools providing real-time mapping of sedimentary formations, bed-boundaries detection, anisotropy determination, and azimuthal resistivity measurements for accurate well placement and formation evaluation, detection of metal cased holes in mature oilfields (Clegg, et al., 2021), and so on.

The UDAR-LWD tools use multi-spacing, multi-component, and multi-frequency induction measurements to implement the look-around the borehole and look-ahead the drill-bit techniques used in geosteering when the targets are relatively far away. Thus, instead of reactively geosteering based on the formation resistivity properties at or behind the drill-bit furnished by conventional LWD tools, these new technologies allow proactively navigating based on the formation resistivities several meters around and/or ahead of the bit so that formation boundaries and secondary targets may be now mapped, allowing for improved planning for future wells (Cunha et al., 2024).

In addition, UDAR-LWD technology opened the possibility to integrate surface seismic data to predict formation change ahead of the bit in real time to make more informed decisions (Mele, et al., 2022).

Figure 1 shows the building blocks for the modern multicomponent induction tools (Triaxial-wireline or UDAR-LWD) which consists of three mutually orthogonal coil transmitters $(T_{x'}, T_{y'}, T_{z'})$ and coil receivers $(R_{x'}, R_{y'}, R_{z'})$ in an arbitrary position ($\theta \neq 0°$; $\emptyset \neq 0°$; $\gamma \neq 0°$) within a basic 1D VTI anisotropic ($\sigma_x = \sigma_y = \sigma_h; \sigma_z = \sigma_v$) layer cake model.

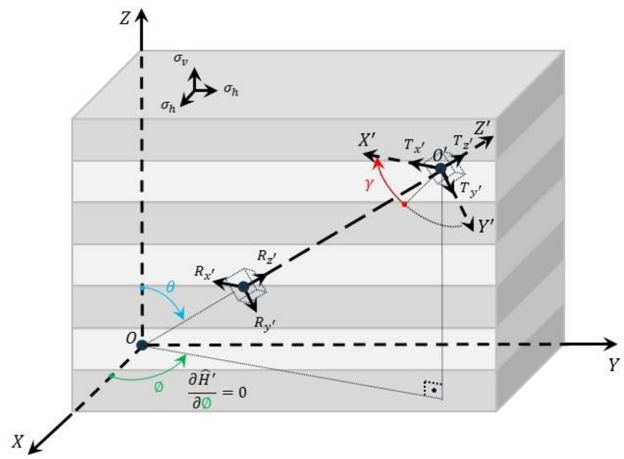

Figure 1 – The building block of the multicomponent induction tool (triaxial-wireline or UDAR-LWD) within a 1D VTI anisotropic layer cake model.

The Table 1 shows the nine triaxial magnetic components in the instrument coordinate system (tool frame) in which its three mutually orthogonal axes $X'Y'Z'$ are aligned with the transmitter coil axes $(T_{x'}, T_{y'}, T_{z'})$ where H_{ij} represents the ith magnetic component due to the jth component of the magnetic dipole source T_j.

Table 1 – The nine magnetic signals of the multicomponent induction tools in arbitrary position showed in the tool frame.

	$T_{x'}$	$T_{y'}$	$T_{z'}$
$R_{x'}$	$H_{x'x'}$	$H_{x'y'}$	$H_{x'z'}$
$R_{y'}$	$H_{y'x'}$	$H_{y'y'}$	$H_{y'z'}$
$R_{z'}$	$H_{z'x'}$	$H_{z'y'}$	$H_{z'z'}$

The three terms of the diagonal $H_{x'x'}$, $H_{y'y'}$ and $H_{z'z'}$ are the direct-coupled signals (parallel source/sensor axes) and they are considered the triaxial main components. The signal $H_{z'z'}$ is in the traditional coaxial coil configuration where the source and receiver axes are aligned with the longitudinal sonde axis. Its magnitude is usually the biggest of all (Zhdanov et al., 2001) since it is predominantly due to the horizontal conductivity σ_h which is higher than the vertical conductivity σ_v in most anisotropic hydrocarbon environments. The signals $H_{x'x'}$ and $H_{y'y'}$ are in the coplanar coil configurations where the source and receiver axes are parallel to each other and perpendicular to the sonde axis.

Kaufman and Ytskovich (2017) show that the reason between the imaginary part of the coaxial signal to one of the coplanar signals, in low frequency and vertical wells, approximates the VTI anisotropy media ratio $\lambda^2 \approx \sigma_h / \sigma_v$.

The remaining off-diagonal six terms, $H_{x'y'}, H_{y'x'}, H_{x'z'}$, $H_{z'x'}$, $H_{y'z'}$, $H_{z'y'}$, are the cross-coupled signals (perpendicular source/sensor axes). These data contain complementary information about anisotropic resistivity, wellbore dipping as well as tool rotation angle around its axis. According to Zhang et al. (2004) the signal-to-noise ratio in these components is very low, mainly in the four Y-related cross-coupling, and, consequently, they have been neglected in 1D inversion codes and have been exploited to provide information only about 3D resistivity structures (Bergeron et al., 2022).

Hong et al., 2014 show the sum of $H_{z'x'}$ and $H_{x'z'}$ furnished a symmetrical and square-looking log which depend only on horizontal conductivities with little nonlinearity. Thus, this new log proposed by them has a small shoulder bed effect and, consequently, much higher vertical resolution than any two signals alone or even the direct coupling signals in horizontally layered formations.

In an actual LWD field situation, the triaxial tool trajectory is a continuous 3D line penetrating a 3D earth's subsurface and, according to Zhang et al. (2004), it involves five angles (formation dip; formation azimuth; wellbore dip; wellbore azimuth; and the instrument roll on its axis) and four coordinate systems (earth; formation; tool; and coils).

Following the most forward modeling codes used for data inversion, for the sake of simplification, we focus on the effects of only three relative angles (Fig. 1) on the nine signals of the triaxial induction tensor: wellbore dip angle θ; wellbore azimuth angle $\emptyset$, as well as the tool rotation angle γ. Thus, just two coordinate systems are necessary to obtain the synthetic data: the medium frame XYZ (unprimed) and the tool frame $X'Y'Z'$ (primed)

In Fig. 1 the dip angle θ and azimuth angle $\emptyset$ of the wellbore are the same of the spherical coordinate system but, the roll angle γ around the Z' tool axis is not so obvious as, according to Zhdanov et al. (2001), it is that which the tool's transverse x'-source dipole makes with the line of intersection of the $X'Y'$ tool plane with the XZ medium plane.

Theory and Method

Our goal here is to investigate the sensitivities of each of the nine triaxial induction signals in relation to the wellbore trajectory angles (θ and $\emptyset$) and the tool rotation angle (γ) around its axis (Fig.1).

This investigation is conducted using a basic 1D layered cake model that includes formations with transverse isotropy (VTI anisotropy). The model also includes an arbitrary wellbore trajectory that penetrates the formations. It is assumed that the borehole and fluid invasion effects are insignificant.

The layered 1D VTI anisotropic problem is formulated using the mathematical tools described by Kaufman and Ytskovich (2017). The analytical solutions are written as integrals of the Hankel transform, which are evaluated numerically using the Quadrature With Extrapolation (QWE) method as presented by Key (2012).

The nine triaxial signals of Table 1 can be organized mathematically in a square matrix (Eq. 01) named by Zhdanov et al. (2001) as magnetic induction tensor $\widehat{H}'$ in the tool coordinate system which is given by:

$$\widehat{H}' = \begin{bmatrix} H_{x'x'} & H_{x'y'} & H_{x'z'} \\ H_{y'x'} & H_{y'y'} & H_{y'z'} \\ H_{z'x'} & H_{z'y'} & H_{z'z'} \end{bmatrix}. \tag{1}$$

These nine magnetic components are computed from analytical formulas for the vertical and horizontal dipole sources directed along the coordinate axes of the formation coordinate system (Eq. 02), chosen to coincide with the main conductivity axes of the 1D VTI anisotropic layer cake model.

$$\widehat{H} = \begin{bmatrix} H_{xx} & H_{xy} & H_{xz} \\ H_{yx} & H_{yy} & H_{yz} \\ H_{zx} & H_{zy} & H_{zz} \end{bmatrix}. \tag{2}$$

We transform the triaxial induction tensor from medium frame XYZ (Eq. 2) to tool frame $X'Y'Z'$ (Eq. 1), or vice-versa, with three relative rotations that are represented mathematically in the overall rotation matrix R in Eq. 03 that allows us to migrate from the simplest case, which is the vertical wellbore without tool rotation ($\theta = \emptyset = \gamma = 0°$), to the more general case which is a deviated wellbore in an arbitrary position ($\theta \neq 0°$; $\emptyset \neq 0°$; $\gamma \neq 0°$) which is given by:

$$\widehat{H}' = R^T \, \widehat{H} \, R. \tag{3}$$

which

$$R = \begin{bmatrix} \cos\theta \cos\emptyset \cos\gamma - \sin\emptyset \sin\gamma & -\cos\theta \cos\emptyset \sin\gamma - \sin\emptyset \cos\gamma & \sin\theta \cos\emptyset \\ \cos\theta \sin\emptyset \cos\gamma + \cos\emptyset \sin\gamma & -\cos\theta \sin\emptyset \sin\gamma + \cos\emptyset \cos\gamma & \sin\theta \sin\emptyset \\ -\sin\theta \cos\gamma & \sin\theta \sin\gamma & \cos\theta \end{bmatrix}. \tag{4}$$

To show the nine triaxial logs in the same track and due to the large difference in magnitude between the main direct signals and the cross-coupling signals, we follow Zhang et al. (2012) and convert the imaginary part of the magnetic induction matrix $\widehat{H}'$ (Eq. 1) to the apparent conductivity matrix $\hat{\sigma}'$ (Eq. 5) with the geometric weighting matrix K (Eq. 6) through a simple element by element product:

$$\hat{\sigma}' = K \cdot \widehat{H}' = \begin{bmatrix} \sigma_{x'x'} & \sigma_{x'y'} & \sigma_{x'z'} \\ \sigma_{y'x'} & \sigma_{y'y'} & \sigma_{y'z'} \\ \sigma_{z'x'} & \sigma_{z'y'} & \sigma_{z'z'} \end{bmatrix}. \quad (5)$$

which

$$K = \begin{bmatrix} K_{x'x'} & K_{x'y'} & K_{x'z'} \\ K_{y'x'} & K_{y'y'} & K_{y'z'} \\ K_{z'x'} & K_{z'y'} & K_{z'z'} \end{bmatrix} = \begin{bmatrix} \frac{8\pi L}{\omega\mu} & \frac{8\pi L}{\omega\mu} & \frac{16\pi L}{\omega\mu} \\ \frac{8\pi L}{\omega\mu} & \frac{8\pi L}{\omega\mu} & \frac{16\pi L}{\omega\mu} \\ \frac{16\pi L}{\omega\mu} & \frac{16\pi L}{\omega\mu} & \frac{4\pi L}{\omega\mu} \end{bmatrix}. (6)$$

Results

We discuss geometrically and numerically the results that show the wellbore azimuthal symmetry of the triaxial induction matrix as well as other angle effects within a five-layer 1D formation model (Fig. 2) given in Wang et al. (2006). This five-layer formation model consists, from top to bottom: 1) a very thick anisotropic shale with horizontal and vertical resistivity of 1.0 and 2.0 ohm-m, respectively; 2) a thinly laminated sand/shale layer with a structural anisotropy with vertical resistivity of 11 ohm-m and horizontal resistivity of 1.9 ohm-m; 3) an oil-bearing isotropic sandstone layer with 50 ohm-m resistivity; 4) an isotropic water-saturated sand with 0.5 ohm-m resistivity, and 5) a very thick isotropic shale of 1.0 ohm-m.

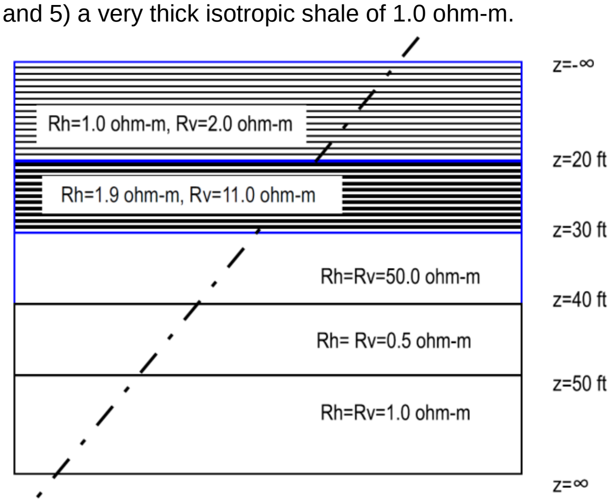

Figure 2 – The 1D formation model (Wang et al., 2006) to verify the effects of the dip and azimuth of the wellbore as well as the tool rotation angle on the triaxial tensor.

In this simplified study, the triaxial logging tool has only one transmitter and one receiver with an offset of 40 in and 20 kHz operating frequency. Following Wang et al. (2006) and Liu, (2017) the triaxial tool crosses the formation layer in three cases:

In the first case, the instrument frame (primed) and medium frame (unprimed) become the same and the medium tensor is equal to the tool tensor since the rotation matrix in Eq. 03 becomes an identity matrix ($R = R^T = I$). Thus, the full apparent conductivity matrix (Eq. 05) reduces to diagonal matrix in Eq. 07.

$$\hat{\sigma}' = \begin{bmatrix} \sigma_{x'x'} & 0 & 0 \\ 0 & \sigma_{y'y'} & 0 \\ 0 & 0 & \sigma_{z'z'} \end{bmatrix} = \begin{bmatrix} \sigma_{xx} & 0 & 0 \\ 0 & \sigma_{yy} = \sigma_{xx} & 0 \\ 0 & 0 & \sigma_{zz} \end{bmatrix}. \quad (7)$$

Fig, 3 shows that in vertical wellbores the two coplanar signals $\sigma_{x'x'}$ and $\sigma_{y'y'}$ are always equal and are generally smaller than that of the coaxial $\sigma_{z'z'}$, except within the isotropic oil-bearing sandstone (third layer), due to their well-known strongest skin effect within the conductive media (Anderson et al., 2002), as well as their high sensibility to the formation vertical conductivities σ_v in the anisotropic layers.

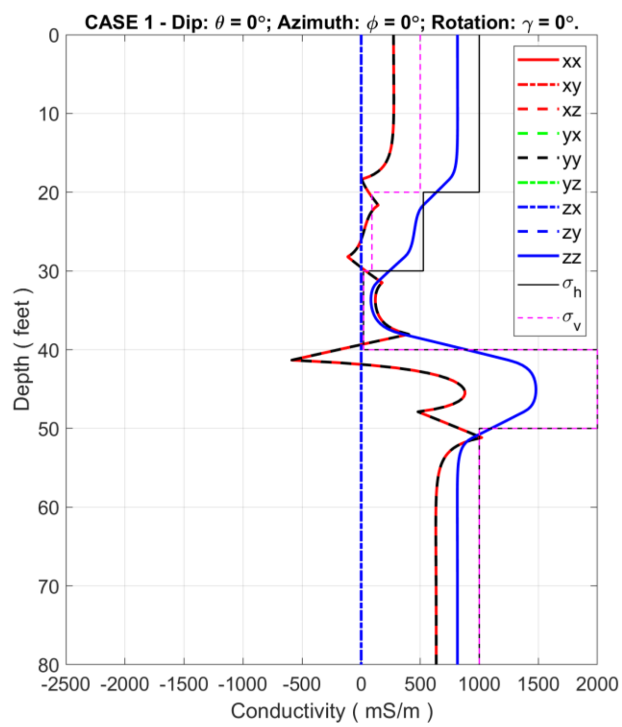

Figure 3 – Case 1: Vertical wellbore where the dip and azimuth wellbore angles, as well as the tool rotation angles are null ($\boldsymbol{\theta} = \emptyset = \boldsymbol{\gamma} = \mathbf{0}$).

The so called "horning" effect in front of the bed-boundaries in both coplanar logs has been shown by Régis et al. (2020) to be associated with the discontinuous current density field parallel to the interfaces between layers, rather than with surface charge build-up from the continuous current across the interface, as was universally accepted since the early 1990s.

The second case is a wellbore at oblique angle ($\theta = 75°$) in the XZ plane, where the wellbore azimuth and tool rotation angles are null ($\emptyset = \gamma = 0°$). Thus, the off-diagonal positions start to appear in the apparent conductivity matrix because the two cross-coupling signals $\sigma_{z'x'}$ and $\sigma_{x'z'}$ are no longer null and indicate the loss of verticality of the wellbore since they are very sensitive to dip changes even at angles close to zero (Zhang et al., 2004).

$$\hat{\sigma}' = \begin{bmatrix} \sigma_{x'x'} & 0 & \sigma_{x'z'} \\ 0 & \sigma_{y'y'} & 0 \\ \sigma_{z'x'} & 0 & \sigma_{z'z'} \end{bmatrix}. \quad (8)$$

The four-remaining Y-related cross-coupling signals remain null ($\sigma_{x'y'} = \sigma_{y'x'} = \sigma_{y'z'} = \sigma_{z'y'} = 0$) because the tool rotation angle is zero ($\gamma = 0$) and, consequently, the Y-antennas (sources or receivers) are normal to the XZ plane and parallel to the VTI model layers.

Fig. 4 shows that all these five signals also suffer the "horning" effect since the H_{xx} and H_{yy} play an important role in their compositions. The two cross-coupling signals $\sigma_{x'z'}$ and $\sigma_{z'x'}$ have a good sensibility to anisotropy. They appear in the VTI anisotropic homogeneous medium (top thick layer) but are zero in the isotropic homogenous medium (bottom thick layer). These two logs differ only in front of the bed boundaries because of the "horning" effect. The four Y-related cross-coupling logs ($\sigma_{x'y'}$, $\sigma_{y'x'}, \sigma_{y'z'}$, $\sigma_{z'y'}$) remain null and show as a straight line because the tool rotation angle is still zero ($\gamma = 0$) and their Y-antennas (sources or receivers) are lined up parallel to the VTI layers model.

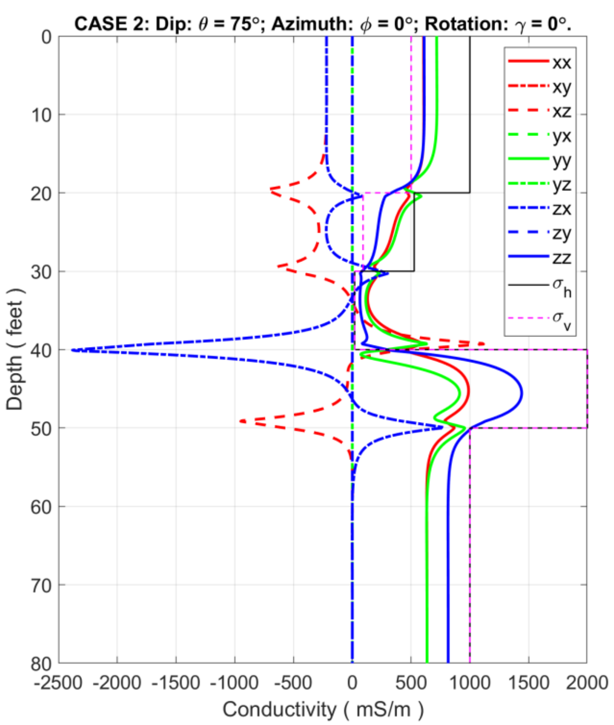

Figure 4 – Case 2: dipping wellbore ($\boldsymbol{\theta} = \mathbf{75}°$) in the $\boldsymbol{XZ}$ coordinate plane where its azimuth and the tool rotation angles are null ($\emptyset = \boldsymbol{\gamma} = \mathbf{0}$).

<u>The third case</u> is also an inclined wellbore ($\theta = 75°$) in the same medium XZ coordinate plane ($\emptyset = 0°$) but now the tool rotation angle is no longer zero ($\gamma = 330°$). The off-diagonal positions in the induction matrix are fully populated because their Y-antennas are no longer parallel to the bed boundaries.

Fig. 5 shows that none of the signals is null, and all present "horning" in front of the bed boundaries. The sensitivity to the anisotropy described to the cross-signals $\sigma_{x'z'}$ and $\sigma_{z'x'}$ is also observed in the four Y-related cross-coupling $\sigma_{x'y'}$, $\sigma_{y'x'}, \sigma_{y'z'}$, $\sigma_{z'y'}$ signals. The two cross-signals $\sigma_{x'y'}$ and $\sigma_{y'x'}$ are the smallest of the induction matrix and they are identical even in terms of "horning" effects.

Comparing the respective logs of Figs. 4 and 5 we verify that the tool rotation angle γ affects all signals, except $\sigma_{z'z'}$, due to the coaxial rotation symmetry in which the source and receiver axes are aligned with the longitudinal tool axis.

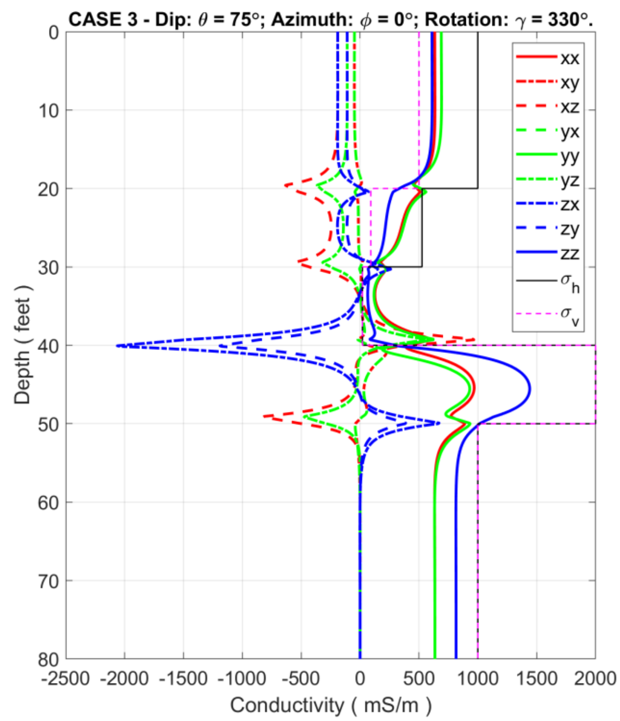

Figure 5 – Case 3: dipping wellbore ($\boldsymbol{\theta} = \mathbf{75}°$) in the coordinate plane $\boldsymbol{XZ}$ where the azimuth angle is null ($\emptyset = \mathbf{0}$) but the tool rotation angles is not ($\boldsymbol{\gamma} = \mathbf{330}°$).

<u>The fourth case</u> is a general situation in which the wellbore and the triaxial tool are in an arbitrary position ($\theta = 75°$, $\emptyset = 30°$; $\gamma = 330°$) outside of any medium coordinate plane (Fig. 6).

The Figs. 5 and 6 are identical and show that if we fix the values of the wellbore dip angle θ and the tool rotation angle γ and vary freely the wellbore azimuth angle $0° \leq \emptyset < 360°$, the relative positions of the nine coil configurations of the triaxial tool remain constant in relation to the VTI anisotropic medium, which is laterally continuous and isotropic.

In a simple VTI homogeneous anisotropic whole space, these signals have closed algebraic formulas (Zhdanov et al., 2001 and Liu, 2017). Therefore, it is possible to check this azimuthal symmetry for any of the nine signals of the triaxial induction matrix.

In the interest of saving space, we showed here only the numerical results. Without losing generality, the interested reader may calculate this derivative for the simplest case that is the coplanar $H_{y'y'}$ signal for $\theta \neq 0°$; $\emptyset \neq 0°$ and $\gamma = 0°$ which is given by:

$$H'_{yy} = (sin\,\emptyset)^2 H_{xx} - sin\,\emptyset\, cos\,\emptyset\, H_{yx} - sin\,\emptyset\, cos\,\emptyset\, H_{xy} + (cos\,\emptyset)^2 H_{yy} \quad (9)$$

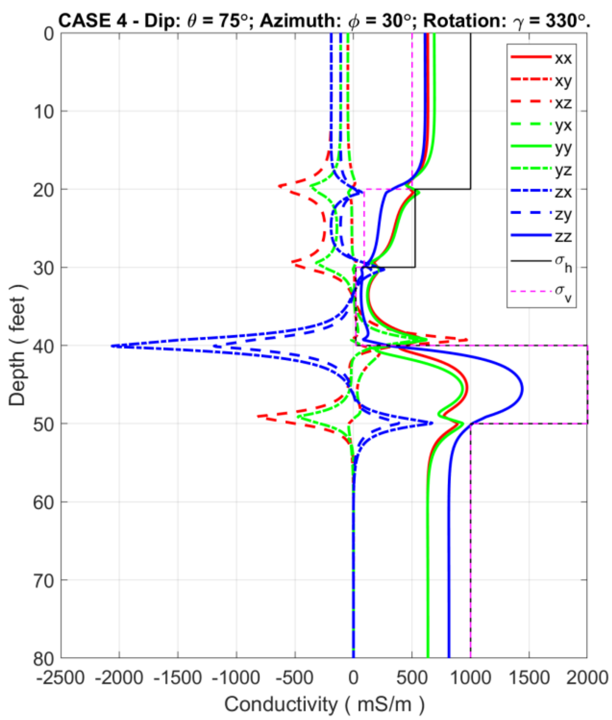

Figure 6 – Case 4: General situation where the dip and azimuth wellbore angles, as well as the tool rotation angles are not null ($\boldsymbol{\theta = 75}°$; $\emptyset = \mathbf{30}°$; $\boldsymbol{\gamma = 330}°$).

Thus, due to this azimuthal symmetry ($\partial\widehat{H}'/\partial\emptyset = 0$), contrary to most works in the available literature as, for example, Zhu et. al, 2023; Liu, 2017; He et. al, 2015, Wang et al., 2006, among others, we recommend, without any loss of generality, ignore the wellbore azimuth angle ($\emptyset = 0$ in Eq. 4) in this type of 1D VTI modelling and consider only the wellbore dip angle θ and the instrument roll angle γ, i.e., positioning the tool just in the XZ coordinate plane, analogous to what Zhdanov et al. (2001) does to the VTI anisotropic whole space.

Conclusion

The numerical responses generated by 1D code show that if we fix the values of the wellbore dip angle and the tool rotation angle and vary freely the wellbore azimuth angle, the relative positions of the nine coil configurations of the triaxial tool remain constant in relation to the VTI anisotropic medium, which is laterally continuous and isotropic.

Most of the available literature works are unclear regarding the description and effects on the triaxial induction tensor of these three relative angles, especially the wellbore azimuth angle, which is often confused with that of the tool rotation angle. Many of these works present these three angles in their illustration models and in the rotation matrix even though their models have perfect rotation symmetry.

To improve understanding and simplify the code for improved efficiency, we strongly advise disregarding the wellbore azimuth angle in this type of 1D modeling. This angle is only significant in situations not having azimuthal symmetry, such as those involving vugs, sand/shale lenses, cross-stratifications, fracture zones, and similar features.

Acknowledgments

The authors thank Petrobras for the financial support of this research through project number 2023/00329-4. Régis and Figueiredo thank the National Council for Scientific and Technological Development (CNPq/Brazil) for the research grants.

References

Anderson, B. I.; Barber, T. & Habashy, T. M. 2002. The interpretation and inversion of fully triaxial induction data; a sensitivity study. 43rd Ann. Logging Sym., Soc. Prof. Well Log. Analysts, paper O.

Clegg, N.; Duriez, A.; Kiselev, V.; Sinha, S.; Parker, T.; Jakobsen, F.; Jakobsen E.; Marchant, D. & Schwarzbach, C. 2021. Detection of offset wells ahead of and around an LWD ultra-deep electromagnetic tool. In: Annual Logging Symposium, 62nd. Virtual event. Anais SPWLA. Paper Number: 0039.
https://doi.org/10.30632/SPWLA-2021-0039

Cunha, A. M. V.; Bohrer, R. W.; Freitas, R. L.; Pedroso, A. R.; Brandão, G. M. S.; Amaral, G. A.; Nakamura, W. Y.; Brasil, F. A. F.; Fonseca, J. P. T.; Koosah, M. P.; Xavier, J. A. P.; Coutinho, C. E. B.; Pessoa, E. C.; Mezzomo, E. H.; Hermida, A. S.; Bernardez, F. P.; Cuadros, G. M.; Matos, L.; Silva, C.; Leveque S. & Salim, D. 2024. Look-Ahead-While-Drilling Technology Assessment for Early Hazards Identification in Presalt Offshore Brazil. In: Annual Logging Symposium, 65th. Rio de Janeiro, Brazil. Anais SPWLA. Paper D.
https://doi.org/10.30632/SPWLA-2024-0060

He Z.; Liu R. C.; Huang K. & Guo C. 2015. A fast algorithm to forward model the triaxial induction logging response in layered transversely isotropic dipping formations. Geophysics, v.80, no 3. http://dx.doi.org/10.1190/geo2014-0321.1

Kriegshäuser, B.; Fanini, O.; Forgang, S.; Itskovich, G.; Rabinovich, M.; Tabarovsky, L. & YU, L. 2000. A new multicomponent induction logging tool to resolve anisotropic formations. In: Annual Logging Symposium, 41st. Dallas, Texas, USA. Anais SPWLA. Paper D.

Liu, C. R., 2017, Theory of Electromagnetic Well Logging. Elsevier, 715 pp.

Mele, M.; Chinellato, F.; Leone, M.; Borahi, M., Tosi, G. & Tveit, J. A. 2022. The Impact of Ultradeep Azimuthal Resistivity Technology on ENI Geosteering Workflow Evolution. In: Annual Logging Symposium, 63rd. Stavanger, Norway. Anais SPWLA. Paper Number: 0044. https://doi.org/10.30632/SPWLA-2022-0044

Régis, C. T.; Carvalho, P. R. & Silva, V. S. 2020. A new look at the causes of “polarization” horns in electromagnetic well logging. Geophysics, v.85, no 6. https://doi.org/10.1190/geo2020-0163.1

Wang H., Barber T., Morriss C., Rosthal R., Hayden R., and Markely M., 2006, Determining anisotropic formation resistivity at any relative dip using a multiarray triaxial induction tool, in: SPE Annual Technical Conference and Exhibition.
https://doi.org/10.2118/103113-MS

Zhang, Z.; Yu, B. & Liu, C. 2012. Investigation of Effects of large dielectric constants on triaxial induction logs. Applied Mathematics, v.3, 1811-1817. http://dx.doi.org/10.4236/am.2012.331246

Zhang, Z.; Yu L.; Kriegshauser, B. & Tabarovsky L. 2004. Determination of relative angles and anisotropic resistivity using multicomponent induction logging data. Geophysics, v.69, no 4.
https://doi.org/10.1190/1.1778233

Zhu G.; Gao M. & Wang B. 2023. A robust inversion of logging-while-drilling responses based on deep neural network. Acta Geophysica (2024) 72:129–139. https://doi.org/10.1007/s11600-023-01080-x